

## Article

# Estimating Groundwater Flow Velocity in Shallow Volcanic Aquifers of the Ethiopian Highlands Using a Geospatial Technique

Hassen Shube <sup>1,2,\*</sup> , Seifu Kebede <sup>3</sup>, Tilahun Azagegn <sup>1</sup>, Dessie Nedaw <sup>1</sup> , Muhammed Haji <sup>2</sup> and Shankar Karuppannan <sup>2</sup> 

<sup>1</sup> School of Earth Sciences, Addis Ababa University, Addis Ababa P.O. Box 1176, Ethiopia; tilahun.azagegn@aau.edu.et (T.A.); dessie.nedaw@aau.edu.et (D.N.)

<sup>2</sup> Department of Applied Geology, School of Applied Natural Sciences, Adama Science and Technology University, Adama P.O. Box 1888, Ethiopia; mohehaji@gmail.com (M.H.); geoshankar1984@gmail.com (S.K.)

<sup>3</sup> School of Agricultural, Earth and Environmental Sciences, Center for Water Resources Research, University of KwaZulu Natal, Pietermaritzburg 3209, South Africa; kebedegurmessas@ukzn.ac.za

\* Correspondence: hassenshube@gmail.com

**Abstract:** The shallow volcanic aquifer is the major rural water supply source in the Ethiopian highlands. A significant number of hand pump wells in these aquifers experience a rapid decline in yield and poor performance within a short period of time after construction. Hence, reliable estimation of groundwater flow velocity is important to understand groundwater flow dynamics, aquifer responses to stresses and to optimize the sustainable management of groundwater resources. Here, we propose the geospatial technique using four essential input raster maps (groundwater elevation head, transmissivity, effective porosity and saturated thickness) to investigate groundwater flow velocity magnitude and direction in the shallow volcanic aquifers of the Ethiopian highlands. The results indicated that the high groundwater flow velocity in the Mecha site, ranging up to 47 m/day, was observed in the fractured scoriaceous basalts. The Ejere site showed groundwater flow velocity not exceeding 7 m/day in the fractured basaltic aquifer and alluvial deposits. In the Sodo site, the groundwater flow velocity was observed to exceed 22 m/day in the fractured basaltic and rhyolitic aquifers affected by geological structures. The Abeshege site has a higher groundwater flow velocity of up to 195 m/day in the highly weathered and fractured basaltic aquifer. In all study sites, aquifers with less fractured basalt, trachyte, rhyolite, welded pyroclastic, and lacustrine deposits exhibited lower groundwater flow velocity values. The groundwater flow velocity directions in all study sites are similar to the groundwater elevation head, which signifies the local and regional groundwater flow directions. This work can be helpful in shallow groundwater resource development and management for rural water supply.

**Keywords:** groundwater flow velocity; geospatial technique; groundwater tools; rural water supply; shallow aquifer; Ethiopia



**Citation:** Shube, H.; Kebede, S.; Azagegn, T.; Nedaw, D.; Haji, M.; Karuppannan, S. Estimating Groundwater Flow Velocity in Shallow Volcanic Aquifers of the Ethiopian Highlands Using a Geospatial Technique. *Sustainability* **2023**, *15*, 14490. <https://doi.org/10.3390/su151914490>

Academic Editor: Dino Musmarra

Received: 2 August 2023

Revised: 11 September 2023

Accepted: 25 September 2023

Published: 5 October 2023



**Copyright:** © 2023 by the authors. Licensee MDPI, Basel, Switzerland. This article is an open access article distributed under the terms and conditions of the Creative Commons Attribution (CC BY) license (<https://creativecommons.org/licenses/by/4.0/>).

## 1. Introduction

Groundwater has a crucial role as a source of water supply in several parts of the world's rural and urban centers. The strategic importance of groundwater for water supply is due to its resilience to more frequent and extreme drought and increased variability in precipitation, sustaining climate change adaptation strategies and groundwater-related ecosystems in sub-Saharan Africa, including Ethiopia [1–3]. Shallow groundwater in sub-Saharan Africa represents a neglected opportunity for promoting small-scale irrigation activities [4]. Since rainfall-dependent agricultural activities have been affected by seasonal variations of climate effects, shallow groundwater can be used as an alternative source for small-scale irrigation. Despite its importance for the water supply, the shallow groundwater

of the Ethiopian highlands has been less investigated. Furthermore, there are unsustainable and low-yielding hand pump boreholes and the rapid transit of contaminated water due to damaged headwork and poor construction that deteriorate groundwater quality [5], decrease aquifer productivity and cause multi-faceted failures of the hand pump boreholes in the shallow aquifers of the Ethiopian highlands [1]. Therefore, understanding groundwater flow velocity has paramount importance in revealing the hydrogeological settings and sustainable groundwater management.

Shallow volcanic aquifers of the Ethiopian highlands were tapped by hand pump wells as a vital source of water supply for significant amounts of people in the remote communities of Ethiopia. However, the shallow volcanic aquifers are characterized by a depletion of water levels due to the response to climate change effects and reduction in groundwater recharge during long dry seasons. Likewise, an increased abstraction of groundwater due to the high population demand for water supply has also caused groundwater depletions [6]. This in turn can affect the hydraulically interconnected aquatic environments dependent on shallow groundwater flow systems.

The shallow volcanic aquifers of the Ethiopian highlands are characterized by moderate to high productivity, and they occur in fractured and weathered tertiary to Quaternary basalts, alluvial deposits and thick weathered regolith [7–11] in the Lake Tana Basin. Similarly, basalt and alluvial deposits are characterized by good productivity, while localized aquifers of rhyolite, trachyte, pyroclastic and welded ignimbrites show a low productivity aquifer system [12] in the Becho Plain and along Awash River banks. Hence, detailed hydrogeological studies of aquifer characteristics and groundwater flow dynamics have a paramount importance for the proper management of shallow volcanic aquifers.

Groundwater flow velocity estimation is fundamentally important in hydrogeological studies for a variety of purposes, including monitoring and predicting contaminant movement and pluming from recharge to the discharge zone, estimating cleanup times, studying recharge, designing permeable reactive barriers (PRBs) and interpreting groundwater movement in regional aquifer systems [13]. Furthermore, measurements of groundwater flow velocity help to identify the dynamics of groundwater flow and its response to stress, optimize water resource management, calibrate groundwater flow and transport modeling and characterize engineering structures associated with groundwater [14]. With the increasing dependence on groundwater resources and geothermal resources, the measurement of groundwater flow velocity magnitude and groundwater flow direction is becoming more and more refined [15].

There are several methods of groundwater flow velocity estimation. The Darcy-based method is a low-cost and effective method that performs groundwater flow velocity estimation at the local and regional scale by using conventional aquifer characterization of water level survey, hydraulic conductivity and effective porosity [16]. The groundwater flow velocity can be estimated by thermal response test [17], radioactive tracer Technetium-99m [18], groundwater flow velocimeter using the point dilution technique to measure in situ groundwater flow velocity [19], the measurement of contact resistance using formation resistivity and solute flow theory related to the change in concentration with the time of a solute to estimate groundwater flow velocity [20] and borehole hydraulic testing to compute flow velocity in un-faulted fractured aquifers [21]. The in-well groundwater flow velocity methods are point dilution methods [22,23]: passive flux meter [24], in-well point velocity probe [25], colloidal borescope [26], heat pulse flowmeter [27] and direct velocity techniques [28]. The  $^{222}\text{Rn}$  isotope is also a proven technique to estimate groundwater flow velocity [29–31]. The estimation of groundwater flow velocity using the geospatial technique has a significant ecological advantage as it uses the measurements of natural groundwater flow systems without introducing artificial tracers. However, another method like the tracer method (e.g., point dilution method) applies artificial tracers which might affect the quality of groundwater along the flow and groundwater-related ecological systems. Similarly, groundwater flow velocity estimation using the natural  $^{222}\text{Rn}$  isotope technique has no effect on the groundwater quality and related aquatic environments,

although it might have inaccurate results due to inappropriate  $^{222}\text{Rn}$  sampling ( $^{222}\text{Rn}$  in the water well and in the aquifer).

The geospatial technique is used to estimate the groundwater velocity at a large scale depending on the four essential maps (groundwater elevation head, effective porosity, saturated thickness, transmissivity) and borehole history, and this method has been conducted in shallow unconsolidated aquifers and fissured-karst aquifers [32,33]. However, groundwater flow velocity estimation in volcanic aquifers has rarely been investigated, particularly in Ethiopian volcanic settings. Therefore, the purpose of this work is to investigate aquifer hydraulic parameters from pumping test data analysis, examine the history of water wells and estimate groundwater flow velocity using a geo-spatial technique in shallow volcanic aquifers of the Ethiopian highlands. This work helps in understanding the groundwater flow dynamics, contaminant pluming, aquifer response to stress, sustainable groundwater development and management in rural water supply and small-scale irrigation activities in shallow aquifers of the Ethiopian highlands.

## 2. Materials and Methods

### 2.1. Geology and Hydrogeology

The study sites (Figure 1) are situated in shallow volcanic aquifers of four major basins of Abay, Awash, Ziway Lake and Ghibe basins. The geology of study sites (Figure 1b–e) comprises volcanic rocks of Oligocene to Quaternary formations. The Mecha site (Figure 1b) is situated in the source region of the Abay Basin. The major geologic units are Quaternary basalts associated with cinder cones, Quaternary alluvium in flat-lying topography and marshy areas and weathered features of tertiary basaltic formation [34,35]. The Miocene basaltic formation is characterized by medium-to-low-productivity fractured aquifers, while Quaternary basalt, alluvium and inter-granular aquifers show high aquifer productivity [7–10,36]. The Ejere site (Figure 1c) is situated in the Awash River Basin. It comprises the Miocene basalt, trachyte and Quaternary alluvial sediments [35,37,38]. The Miocene basalt aquifers are regionally overlain by ignimbrite units and alluvial deposits [12,39–42]. The tertiary trachyte is characterized by low-permeability localized aquifers, while the Quaternary alluvial deposits in the Awash River banks show high productivity.

The Sodo site (Figure 1d) is situated in the Ziway Lake Basin. The geology of this site consists of tertiary weathered basaltic formations intercalated with welded to partially welded pyroclastic flows of ignimbrite, rhyolitic and trachytic lava domes [37,38,43–45] and the Quaternary formations of pyroclastic, lacustrine sediments and the alluvium unit of reworked materials of volcanic origin. The top weathering products were serving as a source of shallow groundwater and springs. The Quaternary basalt and scoria show high productivity as compared to the tertiary basaltic formation, while the trachyte, rhyolite and lacustrine deposits and pyroclastic flow show low productivity [12,39,46,47]. The Abeshege site (Figure 1e) is situated in the Gibe Basin. This site is characterized by tilted and horizontally stratified hexagonal columnar jointing and the thick weathering features of Oligocene basaltic formations. In contrast, the welded pyroclastic flows are characterized by densely welded and lithic fragments associated with rhyolitic lava flows intercalated with ash and unwelded tuffs [37,45,48–52]. The flood basaltic formation and welded to partially welded pyroclastic flows show variable transmissivity and yield of the aquifers where the weathered and fractured units are characterized by good water-bearing formation.

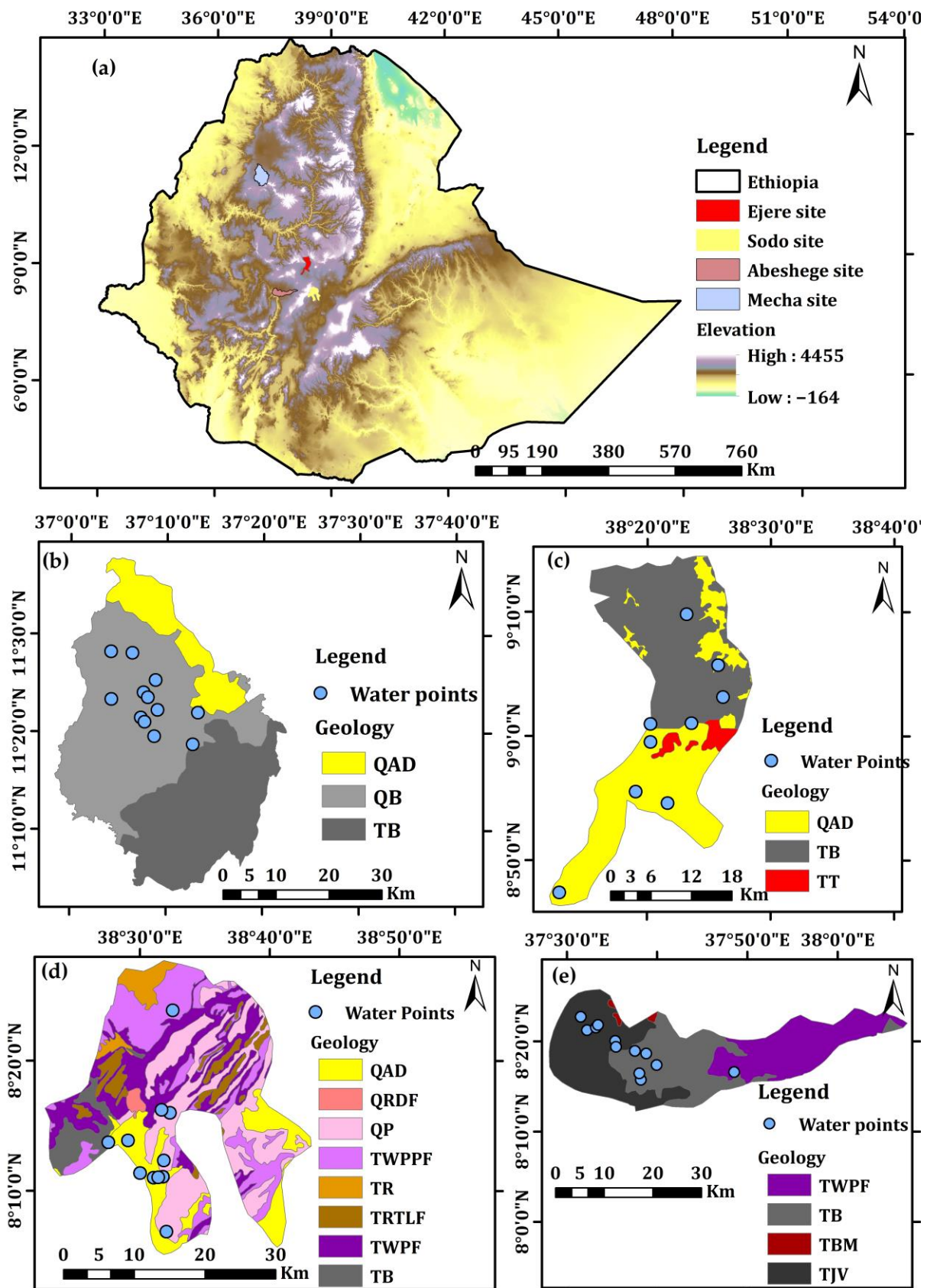


Figure 1. (a) Location maps of four study sites in Ethiopia, (b) geological map of Mecha site, (c) geological map of Ejere site, (d) geological map of Sodo site and (e) geological map of Abeshege site.

The lithological units are: QAD = Quaternary alluvials, lacustrine and soil deposits, QB = Quaternary basalt, TT = tertiary trachyte, QRDF = Quaternary rhyolitic domes and flows, Quaternary pyroclastics, TR = tertiary rhyolite, TRTLF = tertiary rhyolite and trachyte lava flows, TWPPF = tertiary welded to partially welded pyroclastic flows, TWPF = tertiary welded pyroclastic flows, TB = tertiary Miocene flood basalt, TBM = tertiary Oligocene flood basalt and TJV = tertiary volcanics (basaltic and rhyolitic composition) of Oligocene flood basalt.

## 2.2. Pumping Test Data Analysis

In all study sites, the pumping test data were collected from shallow hand pump wells from the Hidden Crises project. The minimum and maximum depths of the boreholes ranged between 18.6 and 84.3 m, respectively. We conducted pumping test data analysis on 42 hand pump boreholes to compute aquifer hydraulic parameters like transmissivity (T), hydraulic conductivity (K) and specific capacity (Sc). The detailed history of water wells, hydraulic parameters and effective porosity are given in the Supplementary Materials. The summary of all the hydraulic parameters obtained from pumping test data analysis and calculated effective porosity is presented in Table 1.

**Table 1.** Summary of water wells history, hydraulic parameters and calculated effective porosity.

Sites		SWL	BH Depth	Saturated Thickness (b)	T (m <sup>2</sup> /day)	Specific Capacity (Sc)	Effective Porosity (Equation (8))
Abeshege	Min	11.17	43.5	11.61	$9.5 \times 10^{-2}$	0.099	0.12
	Mean	35.26	64.1	29.6	$5.33 \times 10^3$	186.8	0.18
	Max	62.16	84.3	53.3	$9 \times 10^2$	845.55	0.26
Ejere	Min	5.94	35.6	17.86	1.17	1.72	0.16
	Mean	16.92	62.66	34.46	$1.19 \times 10^2$	68.28	0.19
	Max	32.82	50.7	47.74	$4.81 \times 10^2$	265.49	0.24
Mecha	Min	2.42	21.75	11.43	$8.35 \times 10^{-1}$	1.96	0.16
	Mean	10.44	44.31	33.21	$4.1 \times 10^2$	327.17	0.21
	Max	23.06	61.34	58.92	$1.61 \times 10^3$	1764.71	0.28
Sodo	Min	10.35	18.6	3.59	$9.07 \times 10^{-1}$	1.52	0.16
	Mean	25.26	46.68	21.06	$7.47 \times 10^1$	38.65	0.19
	Max	52	80	47.12	$3.96 \times 10^2$	163.04	0.23

The pumping test data analysis was carried out using AquiferTest Pro 10 software using a constant discharge rate and recovery test methods. The time against drawdown data were plotted on the log–log scale in the Neuman’s type curve superimposed on the type curve until the data points matched [53]. The Theis Model [54] considers the radial flow presented in the following Equation (1).

$$S(r, t) = \frac{Q}{4\pi T} W(u) \quad (1)$$

where  $s(r, t)$  is the drawdown at the radial distance  $r$  from the well at time  $t$  after pumping commenced,  $u = \frac{r^2 S}{4Tt}$  is the dimensionless quantity that varies with the  $r$  distance from an observation well at time  $t$ ,  $T$  is the transmissivity (m<sup>2</sup>/day) and  $Q$  denotes the discharge rate (m<sup>3</sup>/day),  $S$  is the storativity (dimensionless) and  $W(u)$  is the dimensionless exponential integral known as the well function, which can be approximated as Equation (2):

$$W(u) = \int_u^\infty \frac{e^{-y}}{y} dy = -\gamma - \ln u + u - \frac{u^2}{2.2!} + \frac{u^3}{3.3!} - \frac{u^4}{4.4!} + \dots \quad (2)$$

The well function  $W(u)$  and  $1/u$  are determined from the Theis curve matching technique. The  $T$  and  $S$  were obtained from the time-drawdown curve fitted for both linear and log–log plots to obtain the hydraulic parameters using the following Equations (3) and (4).

$$T = \frac{2.3Q}{2\pi\Delta s} \quad (3)$$

$$S = \frac{2.25Tt_0}{r^2} \quad (4)$$

The behavior and productivity of the water well were determined using the specific capacity as the discharge ratio per unit drawdown expressed as (L/min)/m [55] in Equation (5).

$$Sc = \frac{Q}{S_w} \quad (5)$$

The values of effective porosity of all boreholes were obtained from specific capacity data using the following Equation (6) [56–58].

$$\varphi_i = \frac{\ln\left(\sqrt{\left(\frac{Q}{s}\right)^{0.67} + 1.8}\right)}{5} \quad (6)$$

where  $\varphi_i$  is the dimensionless initial effective porosity,  $Q$  is the water well yield in  $\text{m}^3/\text{day}$ ,  $s$  is the drawdown in  $\text{m}$ ,  $b$  is the saturated thickness in  $\text{m}$  and  $Q/s$  is the specific capacity in  $(\text{m}^3/\text{day})/\text{m}$ . The average effective porosity was obtained from an iterative process of generating the fit solution and re-applying it to the initial effective porosity arrived at in the following Equation (7).

$$\varphi_e = 0.1301 + (0.1544\varphi_i) - (0.0165\varphi_i^2) \quad (7)$$

where  $\varphi_i$  is the initial effective porosity and  $\varphi_e$  is the effective porosity. Equation (7) is re-iterated to obtain the final equation used to calculate effective porosity from only specific capacity, which is determined by using the following Equation (8). This equation is used to estimate effective porosity since the relationship between specific capacity and effective porosity is fitted by  $R^2 = 1.0$  and it is applicable in all hydrogeological environments. However, the main limitation of using this relationship to estimate effective porosity is the inaccuracy of results which arises if the pumping test and water level data are not recent and not properly collected.

$$\varphi_e = 0.15108 \times \left(\frac{Q}{s}\right)^{0.0826} \quad (8)$$

Therefore, for the purpose of this work, effective porosity is determined using Equation (8). The current data show that the specific capacity-based computation of effective porosity uses the logarithmic equation that estimates the initial effective porosity. The correlation analysis shows that  $R^2 = 0.84$  for initial effective porosity against the specific capacity plot. Therefore, the initial effective porosity data were re-iterated to generate the final effective porosity Equation (8), where  $R^2 = 1$ , showing a good fit, as elaborated in the Figure 2.

The seepage velocity is calculated by dividing the Darcy flux by the effective porosity, as shown in Equation (9) [59].

$$V = -\frac{T}{bn_{eff}} \frac{\Delta h}{\Delta s} \quad (9)$$

where  $V$  is groundwater flow velocity ( $\text{m}/\text{day}$ ),  $T$  is transmissivity ( $\text{m}^2/\text{day}$ ),  $b$  is the saturated thickness of the aquifer and  $\frac{\Delta h}{\Delta s}$  is the hydraulic gradient. The hydraulic gradient

estimation, which is represented in the groundwater elevation head, may have uncertainties, such as avoiding closely spaced water well measurements to obtain variations in hydraulic heads, highly permeable sediments showing small differences in the hydraulic head, differing screen lengths in the well which form poor hydraulic interconnections of geologic units, geological barriers or clogged well screens for measurements in the well which are not interconnected, deep groundwater systems or seawater intrusion into the aquifer, which might form different measurements in the well. The groundwater flow velocity estimation considers the homogeneous and isotropic conditions of the aquifer. The results obtained from this method represent the aquifer conditions on a large scale, while the local scale level estimation of groundwater flow velocity needs a single-well method.

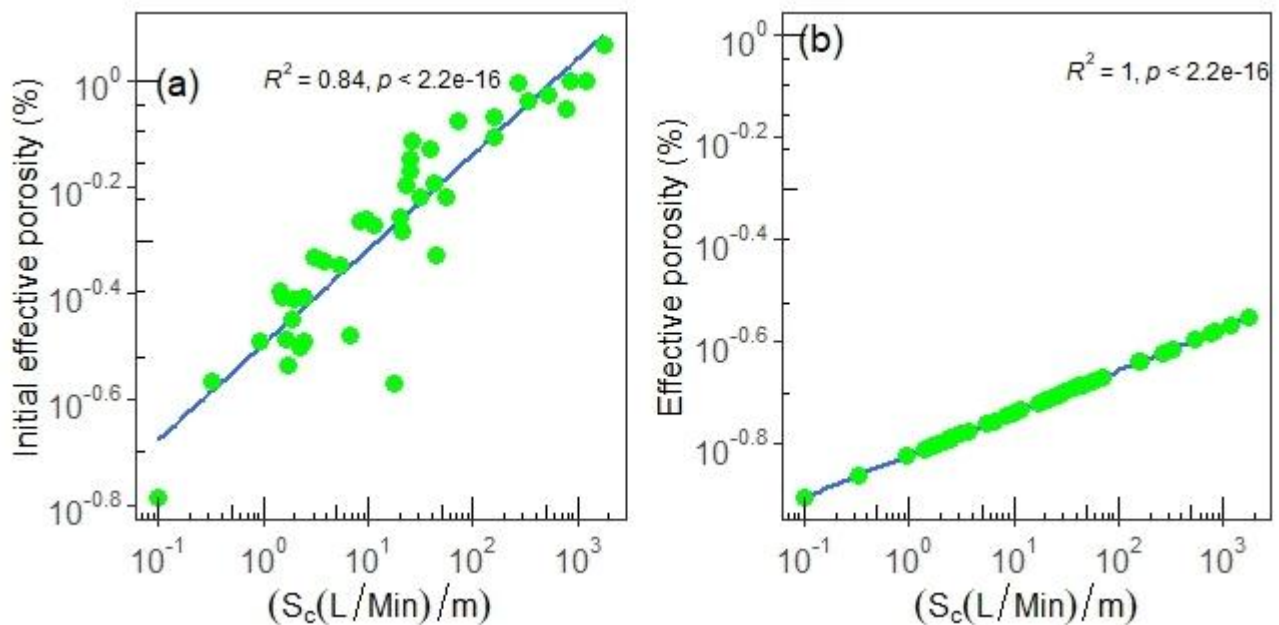


**Figure 2.** (a) The initial effective porosity against specific capacity and (b) the effective porosity against specific capacity plot. The green points show the data and the blue line is the regression line.

### 2.3. Geospatial Technique

The data of the water wells collected from all study sites include information such as water well locations, the static water level in meters below the ground surface (m.b.g.s.) that represents the distance between the ground surface and the static water level in the borehole, the transmissivity of the aquifers ( $\text{m}^2/\text{day}$ ), effective porosity (dimensionless in percentage) and the saturated thickness of the aquifers (m). The homogeneity of the units of the input data was considered during the data processing. The transmissivity value was obtained from pumping test data analysis. The saturated thickness of the aquifer was obtained from the depth of the water table to the bottom of the aquifer. The effective porosity was computed from a specific capacity. In the groundwater flow velocity estimation, three criteria must be fulfilled prior to the use of the input raster maps. These are: (1) the raster maps must have the same extent and cell size, (2) the raster maps must be floating point and (3) the raster maps should be dimensionally homogeneous (i.e., consistent units for all data) [60].

All four raster maps (groundwater elevation head in meters above sea level (masl), transmissivity, effective porosity and saturated thickness) were produced by considering the raster cell size for all four layers in a kriging-type interpolation. The transmissivity, effective porosity and saturated thickness were directly used as inputs in the Arc map spatial analyst toolbox under the groundwater in Darcy velocity command window. Since a static water level raster map cannot be used directly, the command window requires a groundwater head elevation raster map (water table elevation). The groundwater head

elevation raster map was prepared by subtracting the static water level raster map from the digital elevation map (DEM) of the study area, which can be performed by using the Map Algebra/Raster calculator within the spatial analyst tool.

### 3. Results

#### 3.1. Geospatial Analysis of Hydrogeological Features

##### 3.1.1. Groundwater Elevation Head and Water Table Contour Map of all Study Sites

The groundwater elevation head and water table contour maps of all of the study sites are presented in Figure 3a–d. The water table contour maps show the groundwater flow direction in all study sites. In the Mecha site (Figure 3a), the groundwater elevation head and water table contour show a shallow depth in the Quaternary alluvial deposits, reworked soil materials and Quaternary basaltic formations, while the deeper groundwater table is observed in the fractured tertiary basaltic formations. In the Ejere site (Figure 3b), the groundwater table shows a shallow depth in the alluvial deposits situated in the Becho Plain along the Awash River bank, but the deeper groundwater table is observed near the plateau and escarpments. The Sodo site (Figure 3c) groundwater table shows a shallow depth in the areas situated near the bottom of the escarpment and along the rift direction in fractured basalt and Quaternary alluvial deposits. In contrast, a deeper groundwater table depth is observed in the plateau areas in the basaltic and rhyolitic units. In the Abeshege site (Figure 3d), shallow groundwater tables are observed in the Ghibe River discharge zone in the basaltic formations and thick overburden units, while deep groundwater tables are observed in the plateau regions in the fractured basaltic units and welded pyroclastic units.

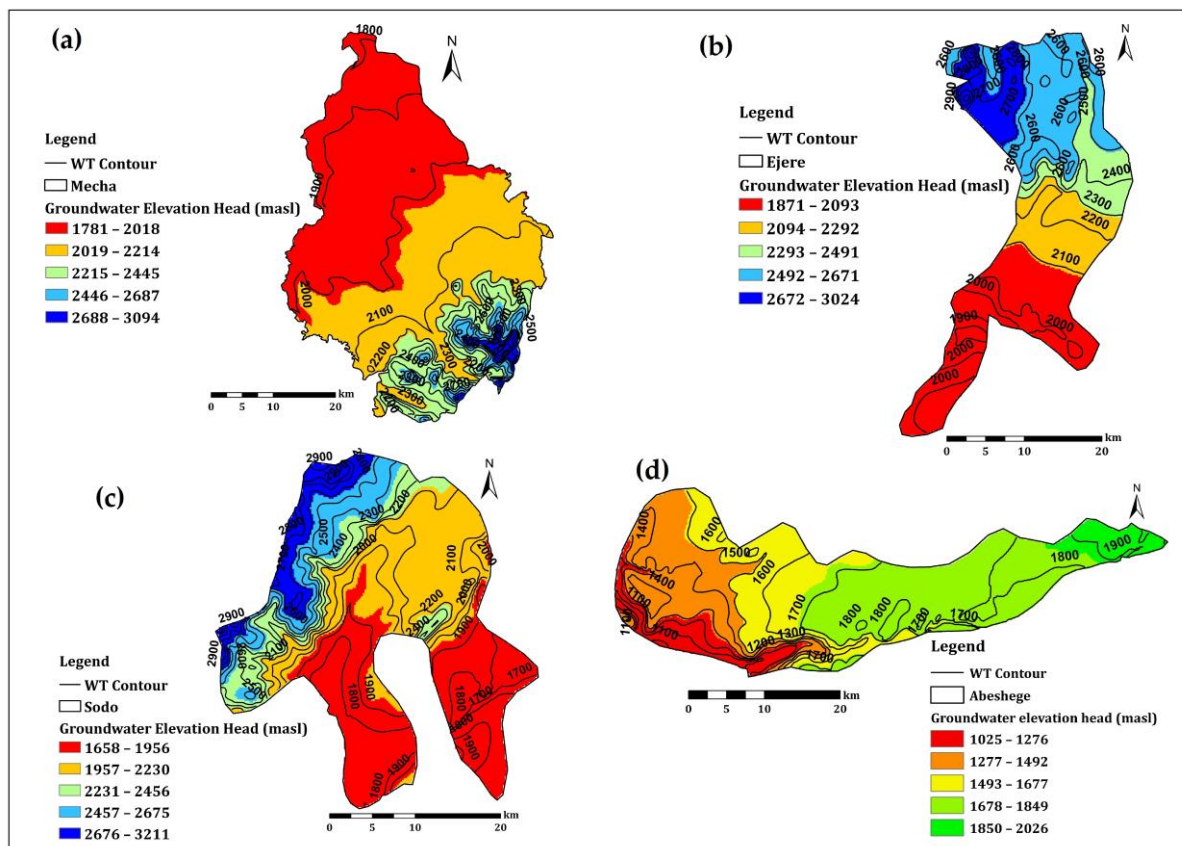


**Figure 3.** Groundwater elevation head and water table contour map depicting groundwater flow direction: (a) Mecha site, (b) Ejere site, (c) Sodo site and (d) Abeshege site.

### 3.1.2. Mecha Site

In the Mecha site, the groundwater elevation head ranged from 1781 to 3094 masl (Figure 4a). The groundwater elevation decreases in the north and northwestern parts of this site, showing the depressed low elevated regions near Lake Tana. Such shallow groundwater elevation is associated with the discharge zone in Lake Tana Graben, whereas the southern and southeastern parts show the elevated regions of the plateau sector showing a deeper groundwater elevation head. Furthermore, the deeper groundwater elevation head is associated with the geological settings that show deep groundwater circulation in a massive fractured basaltic formation at the southern part of the area, while the shallower groundwater elevation is observed in the quaternary alluvial and lacustrine formations near the lake and in the depressed regions.

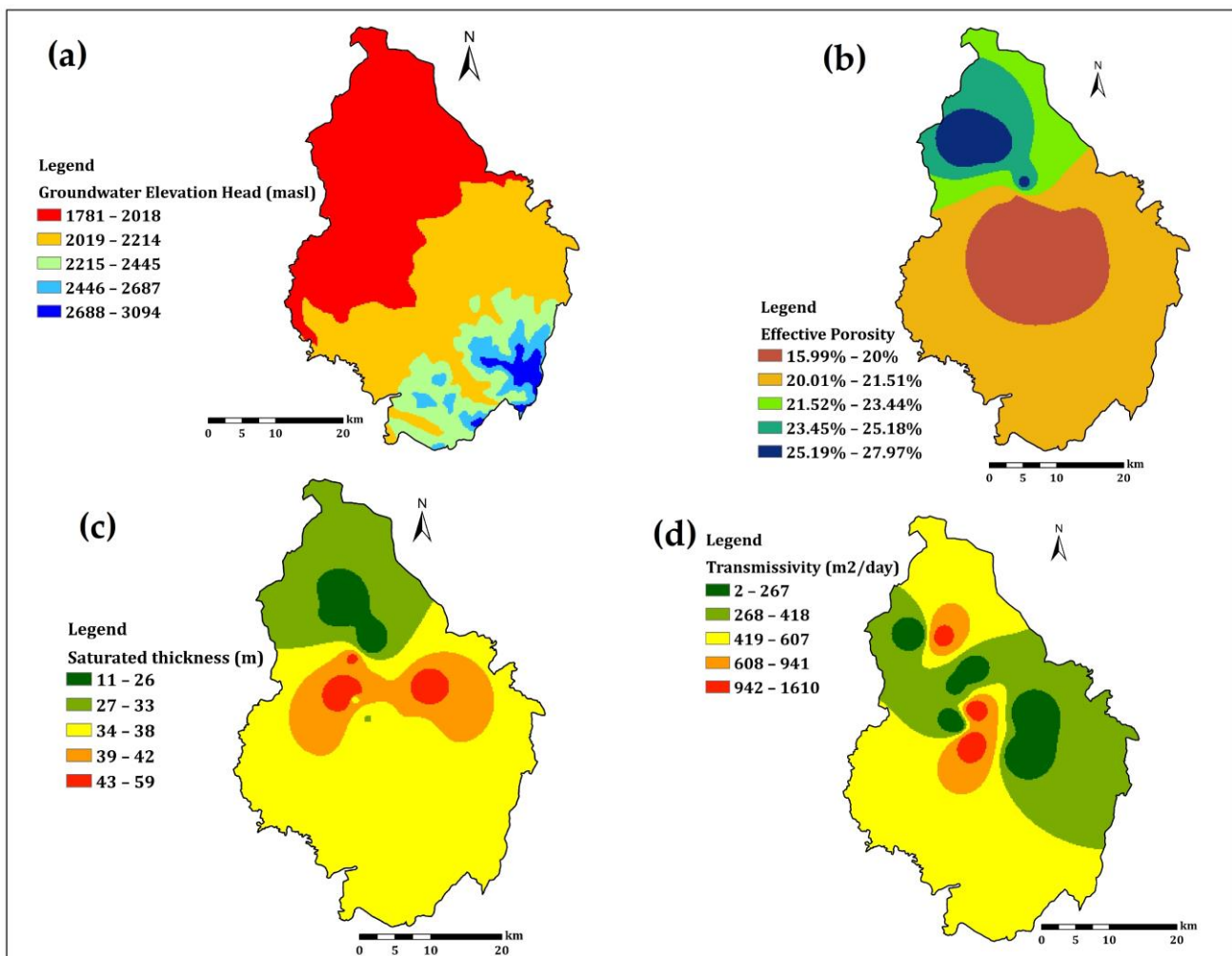


**Figure 4.** Four raster maps of the Mecha site: (a) groundwater elevation head, (b) effective porosity of the aquifer, (c) aquifer saturated thickness and (d) the transmissivity map.

The effective porosity values of this site ranged between 15.99% and 27.97%, as presented in (Figure 4b). The effective porosity is higher in the northern part of the Mecha site, particularly in the Quaternary volcanic formations and in the inter-granular aquifers. In the southern part of the Mecha site, the massive and less-fractured volcanic aquifers showed the lowest value of effective porosity.

The saturated thickness of the Mecha site ranged between 11 and 59 m (Figure 4c). Thick saturated layers are observed in the central part of the area, mainly in the Quaternary basaltic formations. The thin layers of saturated aquifers are found in the lacustrine

alluvial soils near the Lake Tana region. However, the wider areas in the southern part showed intermediate saturated thickness in the fractured tertiary basalt and Quaternary volcanic formations.

The transmissivity of the aquifer in this site, as obtained from the pumping test data analysis, varies from 2 to 1610  $\text{m}^2/\text{day}$  (Figure 4d). This shows that the highest values are at the central part of the study site, while the lowest range of transmissivity was observed at the northwestern and eastern part of the Mecha site. High transmissivity values are associated with the Quaternary basaltic and alluvial deposits, while the lowest transmissivity is observed in the massive basaltic units and lacustrine deposits.

### 3.1.3. Ejere Site

In the Ejere site, the groundwater elevation head was governed by the surface elevation of the study site that ranged from 1876 to 3024 masl (Figure 5a). The highest groundwater elevation head is observed in the northern part of the site where the topographic setting has a significant role mainly in the basaltic formation on the top of the plateau sector, whereas the shallow groundwater elevation heads are observed in the depressed areas of the Becho plain and in the Awash River banks within the alluvial deposits.

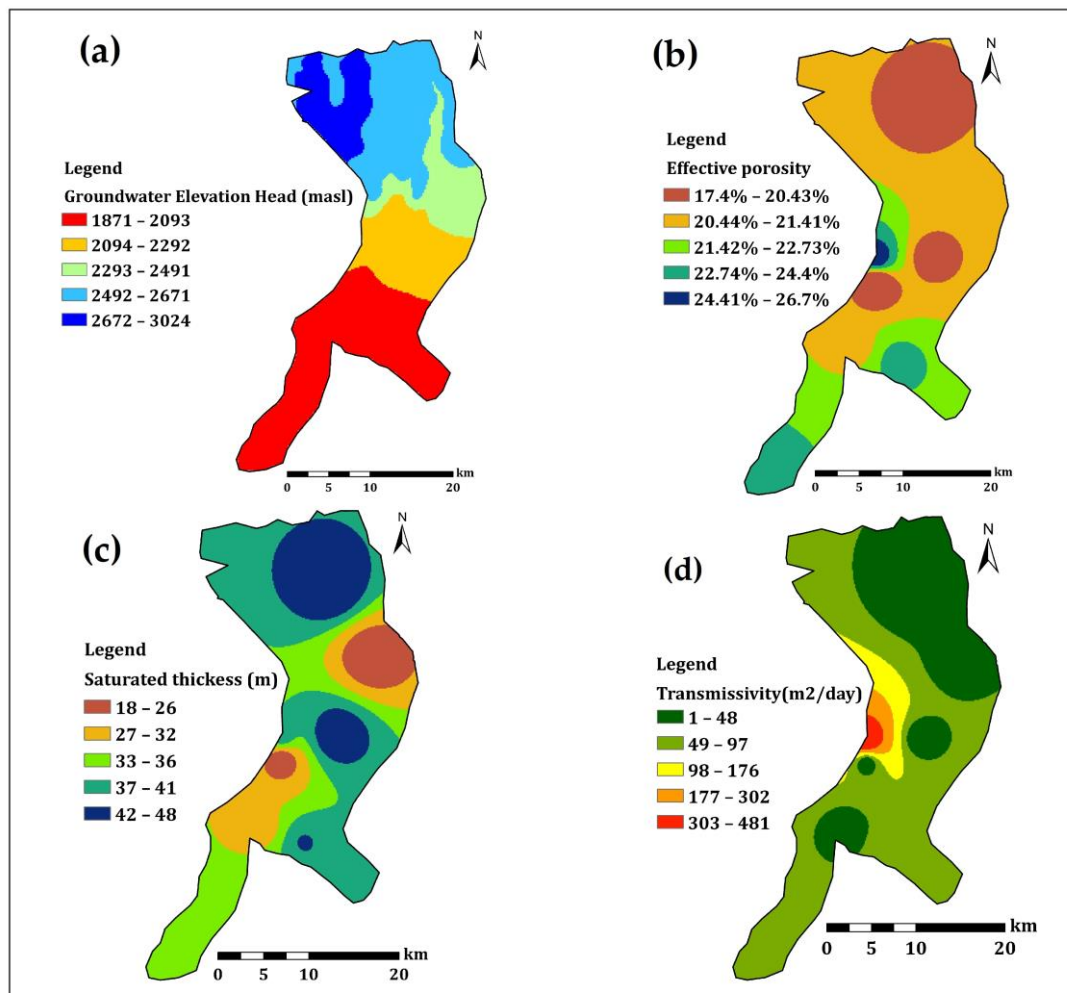


**Figure 5.** Four raster maps of the Ejere Site: (a) groundwater elevation head, (b) effective porosity of the aquifer, (c) aquifer saturated thickness and (d) the transmissivity map.

The effective porosity values varied from 17.4% to 26.7% (Figure 5b). The highest effective porosity is observed at the central part in the fractured basaltic formations affected by the structures and in the southern part of the study site in the highly permeable alluvial

deposits in the Becho Plain and Awash River bank. On the other hand, low values of effective porosities are observed at the northern part of the study site associated with the intermediate to massive basaltic formations.

The saturated thickness of the Ejere site showed values ranging between 18 and 48 m (Figure 5c). The highest value of saturated thickness is observed at the pocket areas of the northern and central parts of the study site, showing the heterogeneity of aquifer thickness distribution due to variations in weathering and fracture units. However, the eastern and the southwestern parts of the region show a saturated thickness of less than 36 m in alluvial deposits and basaltic formations.

The transmissivity values in the Ejere site varied between 1 and 481 m<sup>2</sup>/day (Figure 5d). The highest transmissivity values are observed in the small pocket of the central part of the study site in the tertiary basaltic aquifer, which is highly influenced by the geological structures and topographic effects. In contrast, the northern part showed the lowest transmissivity, which is influenced by the massive tertiary basaltic units, and the central part is identified by less-fractured trachytic deposits.

### 3.1.4. Sodo Site

The Sodo site groundwater elevation head ranged between 1658 and 3211 masl (Figure 6a). The northern and western parts of the site showed deeper groundwater elevation head in the topographically elevated region of Guraghe Mountain dominantly covered by less-fractured tertiary volcanics of the basaltic and welded rhyolitic domes. The southern and eastern parts of the site show shallow groundwater elevation head at the bottom of the escarpment and the depressed areas covered by pyroclastic materials.

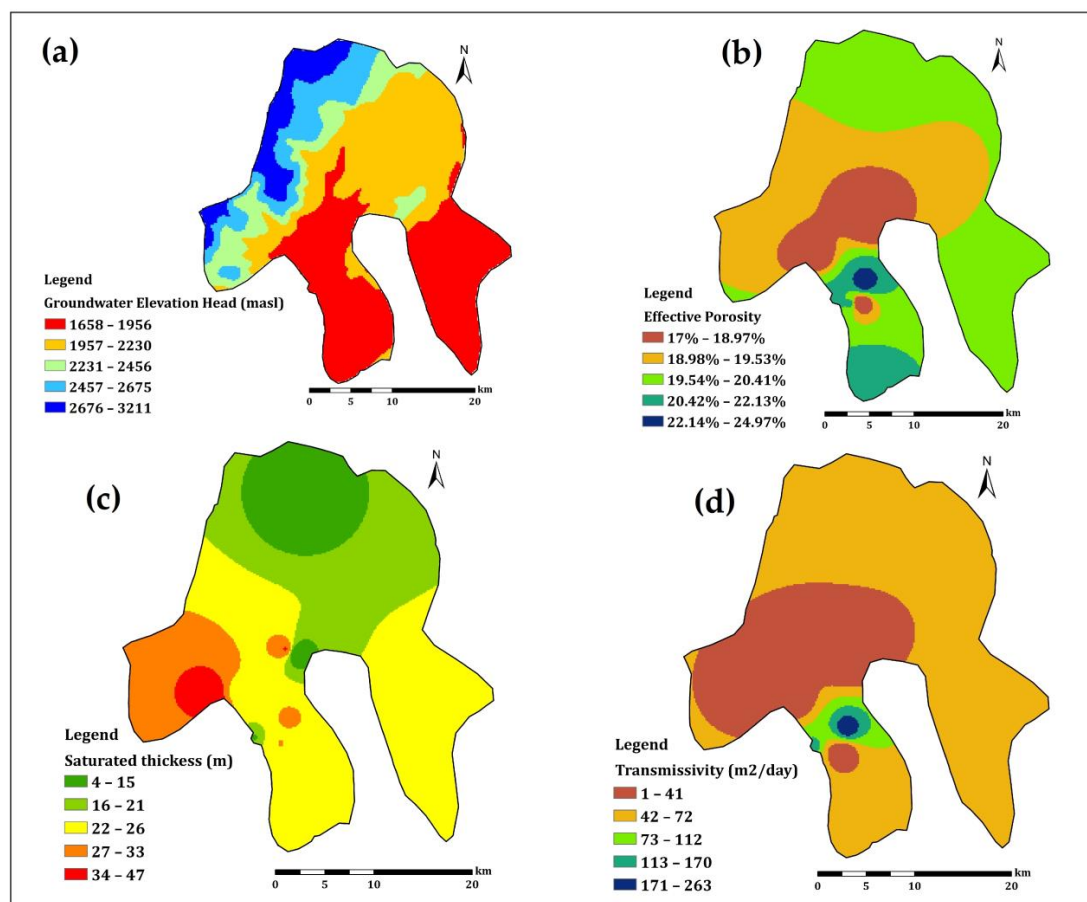


**Figure 6.** Four raster maps of the Sodo site: (a) groundwater elevation head, (b) effective porosity of the aquifer, (c) aquifer saturated thickness and (d) the transmissivity map.

The effective porosity of the Sodo site ranged between 17% and 24.97% (Figure 6b). The low values of effective porosity are associated with the welded and partially welded rhyolite, pyroclastic deposits and less-fractured tertiary basaltic formations. The southern part of the area showed the highest effective porosity associated with fractured and weathered volcanics along the fault escarpment, showing the effects of geological structures.

The saturated thickness of the aquifer in the Sodo site varied from 4 to 47 m (Figure 6c). The southwestern part of the site showed the maximum saturated thickness associated with the fractured and weathered volcanic formations. The eastern and southern parts exhibited a medium range of saturated thickness in partially welded rhyolite and less-fractured rhyolitic and pyroclastic formations, while the northern part showed the lowest saturated thickness of the aquifer on the top of the mountain where the aquifer is shallow at recharge areas.

The transmissivity of the Sodo site ranged between 1 and 263 m<sup>2</sup>/day (Figure 6d). The highest values of transmissivity are observed in the small pocket of the southern part of the area along the fractured zone at the bottom of Guraghe Mountain, which is subsequently affected by geological structures in basaltic and rhyolitic formations. The vast areas of the northern, northwestern and southern parts of the site showed medium-to-low transmissivity in low-permeability welded to partially welded rhyolitic, trachytic formations and pyroclastic materials. Similarly, the top part of Guraghe Mountain showed less-fractured basaltic formations, indicating a low range of transmissivity.

### 3.1.5. Abeshege Site

The groundwater elevation head in the Abeshege site ranged between 1025 and 2026 masl (Figure 7a). The groundwater elevation head is shallower in the western and southwestern parts of the study area, indicating the discharge zone near the margin of river gorge in the Ghibe Basin except in a few areas affected by a series of geological structures that allowed the deeper groundwater flow. The deeper groundwater elevation head in the eastern part of the study area is associated with deep regional groundwater flow from the plateau escarpments to the outlet at the Ghibe Basin.

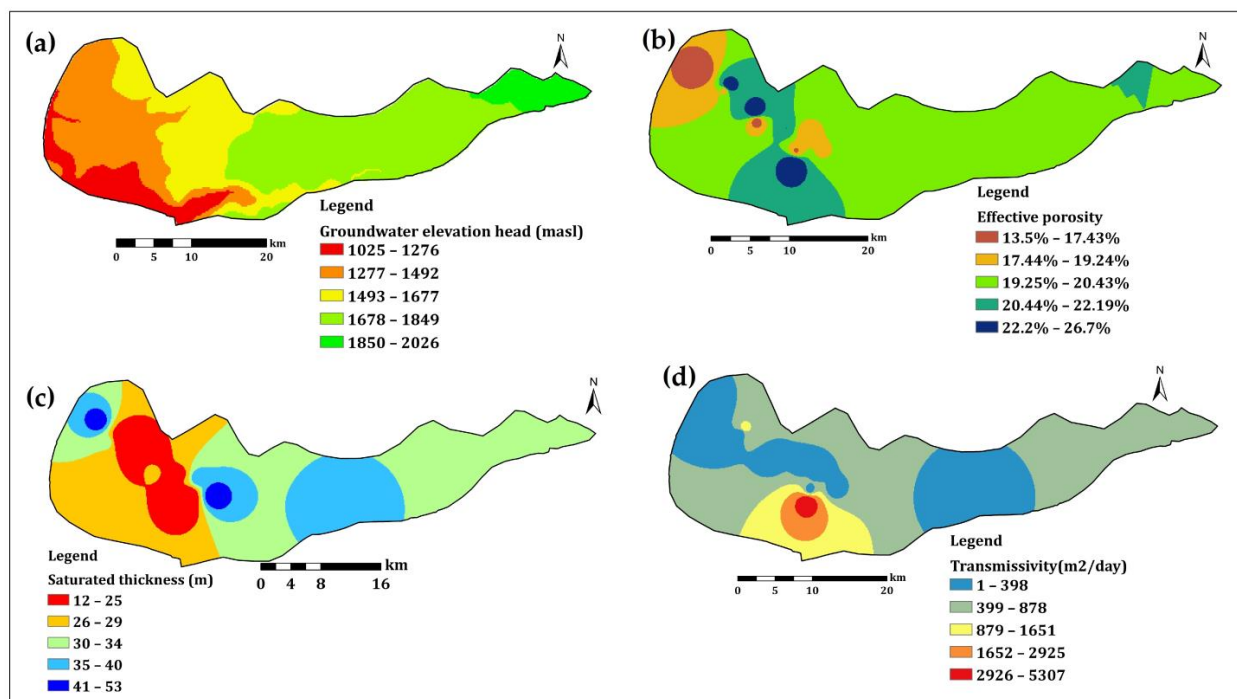


**Figure 7.** Four raster maps of the Abeshege site: (a) groundwater elevation head, (b) effective porosity of the aquifer, (c) aquifer saturated thickness and (d) the transmissivity map.

The effective porosity in the Abeshege site varied from 13.5% to 26.7% (Figure 7b). The highest effective porosity is observed in localized small areas of highly fractured basaltic formation. The western part and small pockets at the center of the study site show the lowest effective porosity in less-fractured and less-weathered tertiary basaltic formations. Welded pyroclastic and massive volcanic formations with low fracture networks showed a medium range of effective porosity.

The saturated thickness of the Abeshege site ranged between 12 and 53 m (Figure 7c). The highest value of saturated thickness was observed at the western periphery and central part of the study site in fractured basaltic formations. The low saturated thickness at the center is associated with the fractured part of the basaltic unit and the top weathered part of the aquifer. The medium range of saturated thickness is in the basaltic and pyroclastic units.

The transmissivity of the Abeshege site varied between 1 and 5307 m<sup>2</sup>/day (Figure 7d). The highest transmissivity value was recorded in the small patchy area affected by the series of geological structures in the basaltic formations. The medium range of transmissivity is associated with the partially welded formation and fractured basaltic units, whereas the low values are observed at the northwestern part and at the central part of the site in welded pyroclastic materials and in massive tertiary basaltic formation.

### 3.2. Groundwater Flow Velocity Estimation

The groundwater flow velocity in the Mecha site ranged between 0 to 47.31 m/day (Figure 8). The highest groundwater flow velocity is observed in the southeastern part of the study site, indicating the effects of elevated topographic features; the geology and geological structures in the tertiary basaltic formations allow an increasing groundwater flow velocity magnitude. Furthermore, such groundwater velocity decreases towards the north in the discharge zone of the Lake Tana Basin. The dominant areas of the study site showed a low range of groundwater flow velocity magnitude mainly in the depressed flat plat plains of the basin except in some volcanic spatter cones sparsely distributed in the site. Furthermore, low groundwater flow velocity is associated with the alluvial and lacustrine deposits. The groundwater flow direction is towards the northwest into Lake Tana, following the regional groundwater flow.

The Ejere site groundwater flow velocity showed values from 0 to 7.47 m/day (Figure 9). The highest groundwater flow velocity magnitude is observed at the central and northwestern parts of the site in fractured and weathered volcanic units affected by geological structures, whereas the dominant part of the study site indicates low values of groundwater flow velocity magnitude in a less-fractured massive tertiary basaltic formation and trachytic units in the northeastern and the depressed Becho Plain that exhibit alluvial deposits. Furthermore, in low groundwater flow velocity regions there are limited effects of geological structures. As compared to all other study sites, the Ejere site shows low ranges of groundwater flow velocity magnitude. The groundwater flow velocity direction is towards the south, following the regional groundwater flow direction from the plateau sectors to the Becho Plain.

The groundwater flow velocity in the Sodo site ranged between 0 and 22.36 m/day (Figure 10). The highest groundwater flow velocity magnitude is observed in the northwestern part of the area where the effects of topography and geological structures are high in the fractured basaltic and rhyolitic formations. The dominant regions of the study site are below 0.79 m/day, showing low groundwater flow velocity controlled by the low permeability welded to partially welded pyroclastic materials, rhyolite, trachyte and the low extent of less-fractured basaltic units. Furthermore, a few areas in the southern part also exhibit low permeability in lacustrine deposits. The groundwater flow velocity direction also indicates the regional groundwater flow direction from Guraghe Mountain to the Rift floor.

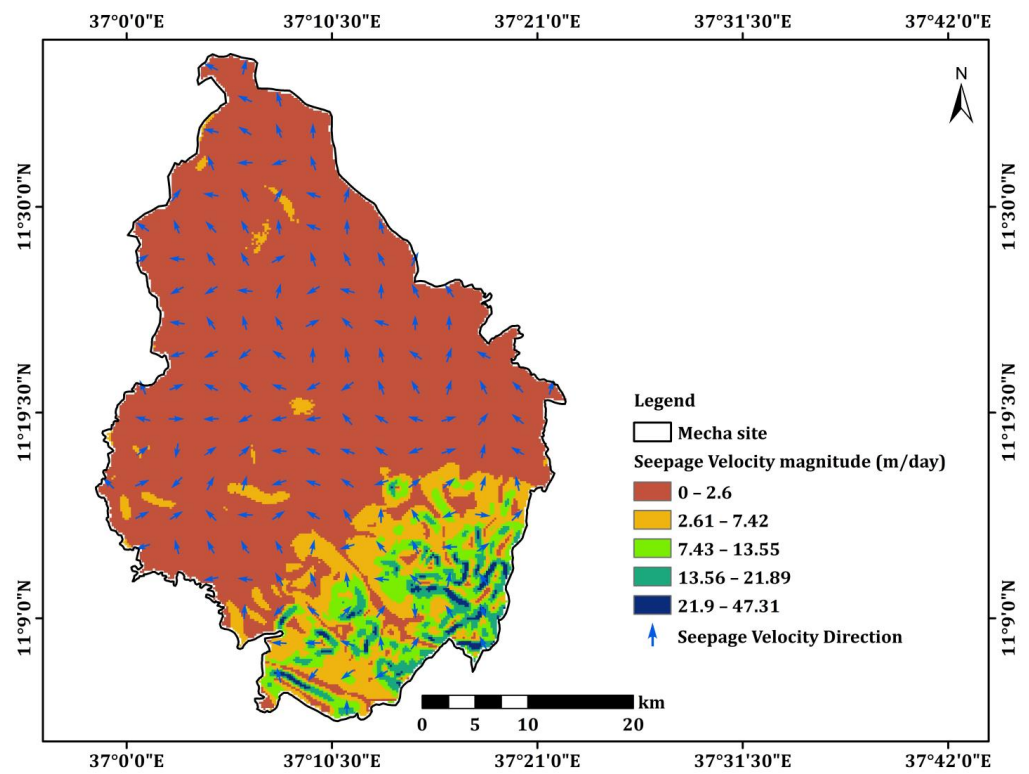


Figure 8. The groundwater flow velocity magnitude and direction of the Mecha site.

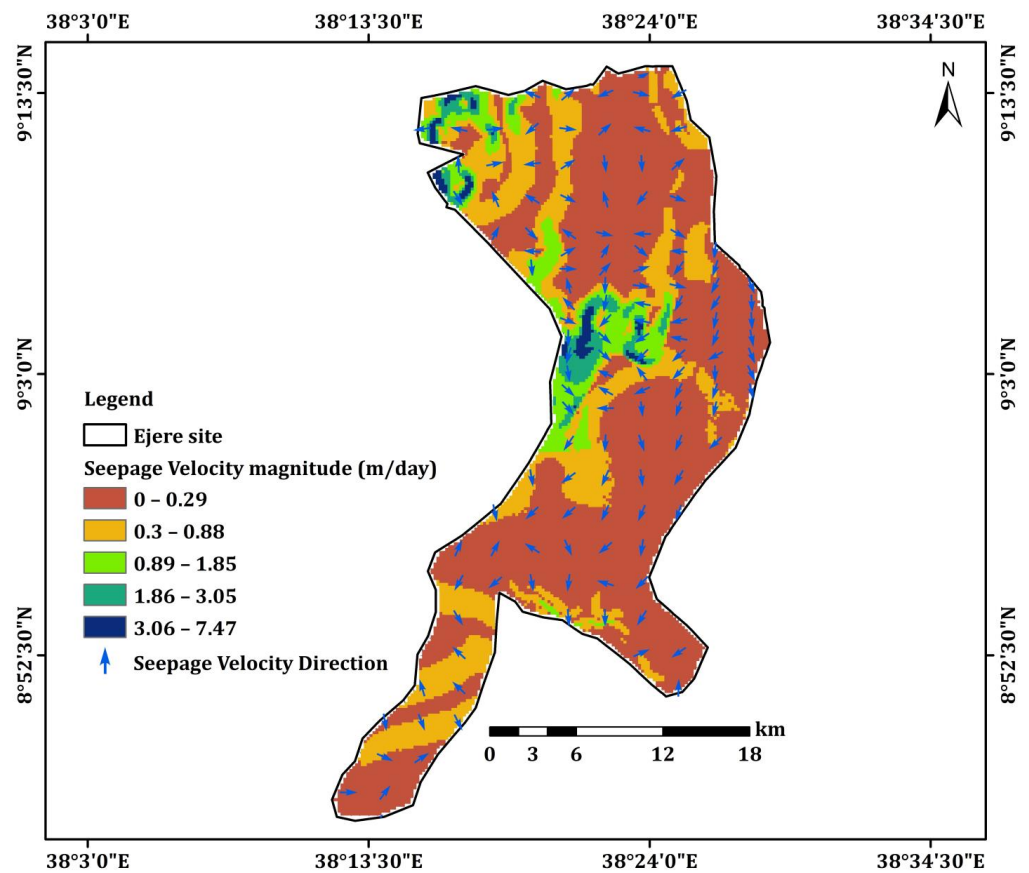


Figure 9. The groundwater flow velocity magnitude and direction of the Ejere site.

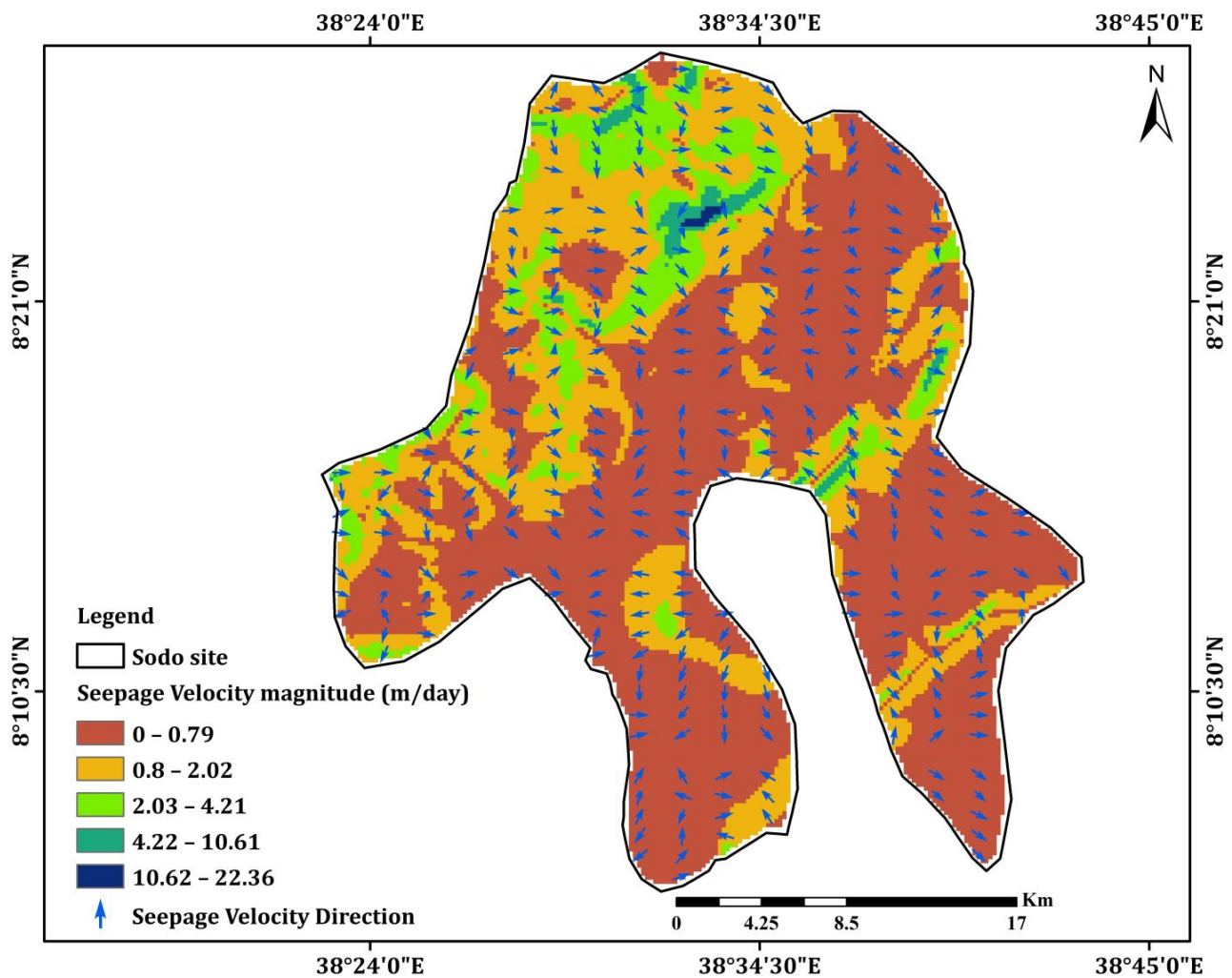
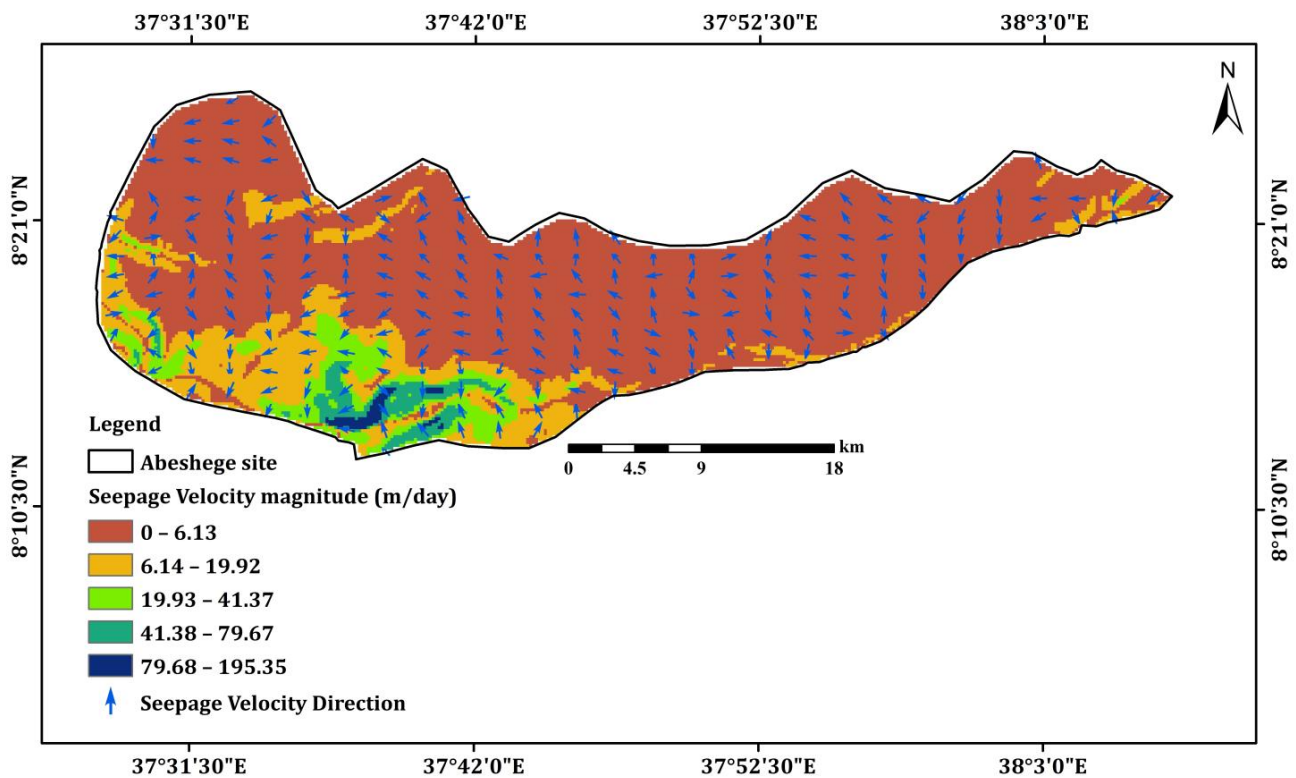


Figure 10. The groundwater flow velocity magnitude and direction of the Sodo site.

The Abeshege site groundwater flow velocity ranged between 0 and 195.35 m/day (Figure 11). The highest groundwater flow velocity magnitude at the southern part of the site is observed in fractured tertiary basaltic units where the effects of topographic features and geological structures are high. Furthermore, such a high-velocity region is situated near the discharge zone of the Ghibe Basin, exhibiting the incising of deep gorges associated with a series of structural networks. However, the dominant regions of this study site in partially welded pyroclastic flows and tertiary basaltic formations with low fracture networks showed a groundwater flow velocity magnitude below 6.13 m/day. The groundwater flow velocity direction is towards the west and the southwest to the Ghibe Basin, following the regional flow system.



**Figure 11.** The groundwater flow velocity magnitude and direction of the Abeshege site.

#### 4. Discussion

##### 4.1. Geospatial Technique in Groundwater Flow Velocity Estimation

Shallow volcanic aquifers are the most reliable water resource that serve most of the Ethiopian volcanic highlands. However, such strategic resources are susceptible to seasonal climatic effects related to the nature of rainfall, contaminations due to unprotected hand pump wells and wastewater discharge in urban areas and stress associated with over-pumping lowering groundwater levels [1,2,61]. The groundwater flow velocity estimation in the shallow volcanic aquifers has vital importance in characterizing the aquifer response to seasonal changes, groundwater flow dynamics and contaminant transport and in optimizing groundwater flow modeling. Previous studies reveal that there has been no investigation on groundwater flow velocity estimation in the Ethiopian shallow volcanic aquifers. The current work is conducted in shallow volcanic aquifers systematically selected from major basins to estimate groundwater flow velocity. The geospatial technique conducted in this work was successfully applied in shallow volcanic aquifers to estimate groundwater flow velocity magnitude and direction.

In the Mecha site, high groundwater elevation head show a significant correlation with high groundwater flow velocity. The groundwater flow velocity shows a similar trend to transmissivity in areas surrounding the Koga Dam. The transmissivity and effective porosity in the depressed plain near Lake Tana are controlled by Quaternary deposits, shallow water levels in the discharge zone, the hydraulic interconnection of surface water with groundwater and irrigation return flow. The higher range of transmissivity and effective porosity are associated with the highly permeable Quaternary basalt aquifer, while the medium-to-low range of transmissivity and effective porosity are associated with tertiary basalt, Quaternary reworked soil and lacustrine deposits. The shallow aquifer saturated thickness is associated with the nature of the shallow water table in the Koga Dam irrigation return flow effect and effects of the discharge zone. These results are in agreement with the previous investigations in the Lake Tana Graben [7,8,10,36].

In the Ejere site, groundwater flow velocity magnitude shows a similar trend with groundwater elevation head, effective porosity and aquifer transmissivity. The ground-

water elevation head is controlled by surface topographic elevation, which shows higher values at the plateau and escarpment region of the site and low values around Becho Plain. The effective porosity is higher in the permeable thick alluvial aquifer of Becho Plain near the Awash River bank, while the effective porosity is low in the massive basaltic and trachytic formations. Similarly, high transmissivity is associated with the fractured tertiary basalt and Quaternary alluvial deposits, while the low transmissivity value is associated with the massive less-fractured basalt and trachytic units. As compared to all other study sites, the Ejere site is characterized by a very low range of groundwater flow velocity magnitude. This might be associated with the less-fractured and less-weathered tertiary basalt and trachytic units. This result is in agreement with previous works conducted in the Upper Awash Basin [12,39,40].

In the Sodo site, high groundwater flow velocity in the Guraghe Mountain range is controlled by geological structures and topographic effects. However, low groundwater flow velocities in all other regions of the Sodo site are characterized by the nature of hydro-stratigraphic units of pyroclastic, rhyolites, trachytic and lacustrine deposits. The groundwater flow velocity and transmissivity show a similar trend of low-to-medium range, which indicates the nature of pyroclastic and lacustrine deposits. The higher effective porosity and transmissivity are associated with the fractured and weathered basalt, rhyolite and alluvial deposits of the high-permeability aquifer, while the lower value is associated with the massive less-fractured rhyolite domes and basaltic formations of the escarpment and the top of Guraghe Mountain.

In the Abeshege site, groundwater flow velocity shows a similar trend with effective porosity and aquifer transmissivity. The highest value of groundwater flow velocity and transmissivity are observed in the fractured and weathered basaltic formation as compared to the other three sites. The high values of groundwater elevation head are controlled by the regional hydraulic gradient and topographic settings surrounding the Ghibe Basin discharge zone. The highly weathered and fractured basaltic unit is characterized by the highest transmissivity and groundwater flow velocity, while the welded pyroclastic deposits show slightly medium-to-low transmissivity and groundwater flow velocity. Furthermore, this site is known for the large tributary rivers of the Ghibe, such as Wabe and Walga, that cross through this study area and wide agricultural fields.

Groundwater flow velocity is estimated to be orders of magnitude higher in fractured media compared to granular media based on aquifer settings like sand (0.1 to 1 m/day), sand and gravel (0.1 to 10 m/day), fractured rock (1 to 100 m/day) and Karst (1 to 500 m/day) [62,63]. The estimated groundwater flow velocity results in the current work are in agreement with the high groundwater flow velocity magnitude in fractured aquifers and low-velocity magnitude in intergranular and alluvial sediments. Similarly, this work shows the results of effective porosity, which are in agreement with the previous work regarding granular media and fractured rocks [64].

#### *4.2. Importance of Groundwater Flow Velocity Estimation in Groundwater Resource Management*

Groundwater flow velocity estimation is important to understand the nature of aquifer productivity, the sustainability of groundwater resources, groundwater flow dynamics, engineering structures associated with groundwater, hydrogeochemical evolution and contaminant transport, groundwater responses to stress, optimizing water resources management and calibrating groundwater flow models [14]. The use of groundwater flow velocity provides essential information to predict the arrival times of contaminants, groundwater mixing, residence times and contaminant mass flux across boundaries at various aquifers and surface water bodies [15,16,65]. Various groundwater flow velocity estimation methods have been conducted based on the single borehole applied [65–69] and environmental tracer test [29,31], direct velocity measurement [26,28,70] and regional scale level Darcy-based and geospatial methods [32,33,71,72].

Geospatial-based groundwater flow velocity estimation can be applied in shallow volcanic aquifers which in turn play a vital role in groundwater resource management,

mainly for hand pump wells in rural water supplies. Therefore, the geospatial technique can be a promising tool to estimate large-scale groundwater flow velocity in the shallow volcanic aquifers of the Ethiopian highlands. The present work would help to practice conducting the method in many other parts of Ethiopian basins at different levels. However, the major challenge is the scarcity of hydraulic parameters data in various basins due to the expensive nature of conducting pumping tests mainly during post-water well construction.

## 5. Conclusions

Shallow volcanic aquifers of the Ethiopian highlands (Mecha, Ejere, Sodo and Abeshege sites) were systematically selected to estimate groundwater flow velocity by using the geospatial technique. The pumping test data analysis was conducted to compute hydraulic parameters (T, K and Sc) and borehole history (depth, static water level and drawdown), and four input raster maps (groundwater elevation head, effective porosity, aquifer saturated thickness and transmissivity maps) were compiled to estimate output resultant maps of groundwater flow velocity magnitude and direction.

The groundwater flow velocity in the selected sites varied between 0 to 47.31, 0 to 7.47, 0 to 22.36 and 0 to 195.35 m/day in Mecha, Ejere, Sodo and Aeshege, respectively. The Abeshege site showed the highest transmissivity and groundwater flow velocity as compared to the other three sites. This is associated with a thick fractured and weathered basaltic aquifer. In the Mecha site, the groundwater flow velocity of the aquifer shows slightly higher values next to the Abeshege site, which is associated with Quaternary basaltic formation and alluvial deposits in the Lake Tana Graben. In the Sodo site, the groundwater flow velocity shows a medium range of distribution in the pyroclastic and lacustrine deposits as compared to other sites, except in a few pocket areas of higher velocity controlled by rugged topography and geological structures. In the Ejere site, groundwater flow velocity shows the lowest value as compared to all other sites in less-fractured and weathered basaltic and trachytic aquifers, while slight increments of groundwater velocity magnitude are observed in the thick alluvial deposits of the Becho Plain.

This work has significant importance in supporting other methods of groundwater flow velocity. Groundwater flow velocity estimation has an important role in understanding groundwater resource management, the sustainability of groundwater resources, groundwater flow dynamics and contaminant transport. Thus, we recommend employing this method for understanding the groundwater resources of shallow volcanic aquifers of the Ethiopian highlands, which serve as a major source of rural water supply.

**Supplementary Materials:** The following supporting information can be downloaded at: <https://www.mdpi.com/article/10.3390/su151914490/s1>, Table S1: Water wells' history, hydraulic parameters and calculated effective porosity.

**Author Contributions:** Conceptualization, H.S. and S.K. (Seifu Kebede); methodology, H.S., T.A. and D.N.; software, H.S., S.K. (Shankar Karuppunnan) and M.H.; validation, H.S., S.K. (Seifu Kebede) and T.A.; formal analysis, H.S.; investigation, H.S. and T.A.; resources, H.S. and S.K. (Seifu Kebede); data curation, H.S. and D.N.; writing—original draft preparation, H.S.; writing—review and editing, H.S., S.K. (Seifu Kebede), T.A., D.N., M.H. and S.K. (Shankar Karuppunnan). All authors have read and agreed to the published version of the manuscript.

**Funding:** This research received no external funding.

**Institutional Review Board Statement:** Not applicable.

**Informed Consent Statement:** Not applicable.

**Data Availability Statement:** Data used in this work are presented in the Supplementary Materials.

**Acknowledgments:** We thank the editor and the anonymous reviewers for their helpful comments in improving the quality of the manuscript. The authors wish to thank the School of Earth Sciences of Addis Ababa University for supporting the field logistics. A special thanks to the Hidden Crises Project for providing us with the pumping test data of hand pump wells.

**Conflicts of Interest:** The authors declare no conflict of interest.

## References

- Macdonald, A.M.; Bell, R.A.; Kebede, S.; Azagegn, T.; Yehualaeshet, T.; Pichon, F.; Young, M.; McKenzie, A.A.; Lapworth, D.J.; Black, E.; et al. Groundwater and resilience to drought in the Ethiopian highlands. *Environ. Res. Lett.* **2019**, *14*, 095003. [[CrossRef](#)]
- MacAllister, D.J.; MacDonald, A.M.; Kebede, S.; Godfrey, S.; Calow, R. Comparative performance of rural water supplies during drought. *Nat. Commun.* **2020**, *11*, 1099. [[CrossRef](#)]
- Taylor, R.G.; Scanlon, B.; Döll, P.; Rodell, M.; Van Beek, R.; Wada, Y.; Longuevergne, L.; Leblanc, M.; Famiglietti, J.S.; Edmunds, M.; et al. Ground water and climate change. *Nat. Clim. Chang.* **2013**, *3*, 322–329. [[CrossRef](#)]
- Gowing, J.; Walker, D.; Parkin, G.; Forsythe, N.; Haile, A.T.; Ayenew, D.A. Can shallow groundwater sustain small-scale irrigated agriculture in sub-Saharan Africa? Evidence from N-W Ethiopia. *Groundw. Sustain. Dev.* **2020**, *10*, 100290. [[CrossRef](#)]
- Banks, E.W.; Cook, P.G.; Owor, M.; Okullo, J.; Kebede, S.; Nedaw, D.; Mleta, P.; Fallas, H.; Gooddy, D.; John MacAllister, D.; et al. Environmental tracers to evaluate groundwater residence times and water quality risk in shallow unconfined aquifers in sub Saharan Africa. *J. Hydrol.* **2021**, *598*, 125753. [[CrossRef](#)]
- Fenta, M.C.; Anteneh, Z.L.; Szanyi, J.; Walker, D. Hydrogeological framework of the volcanic aquifers and groundwater quality in Dangila Town and the surrounding area, Northwest Ethiopia. *Groundw. Sustain. Dev.* **2020**, *11*, 100408. [[CrossRef](#)]
- Mamo, S. Integrated Hydrological and Hydrogeological System Analysis of the Lake Tana Basin, Northwestern Ethiopia. Ph.D. Thesis, Addis Ababa University, Addis Ababa, Ethiopia, 2015; Volume 263.
- Nigate, F.; Van Camp, M.; Yenehun, A.; Belay, A.S.; Walraevens, K. Recharge-discharge relations of groundwater in volcanic terrain of semi-humid tropical highlands of Ethiopia: The case of infranz springs, in the upper blue Nile. *Water* **2020**, *12*, 853. [[CrossRef](#)]
- Walker, D.; Parkin, G.; Gowing, J.; Haile, A.T. Development of a hydrogeological conceptual model for shallow aquifers in the data scarce upper Blue Nile basin. *Hydrology* **2019**, *6*, 43. [[CrossRef](#)]
- Nigate, F.; Ayenew, T.; Belete, W.; Walraevens, K. *Overview of the Hydrogeology and Groundwater Occurrence in the Lake Tana Basin, Upper Blue Nile River Basin*; Springer: Cham, Switzerland, 2017; pp. 77–91.
- Kassune, M.; Tafesse, N.T.; Hagos, M. Characteristics and Productivity of Volcanic Rock Aquifers in Kola Diba Well Field, North-central Ethiopia. *Univers. J. Geosci.* **2018**, *6*, 103–113. [[CrossRef](#)]
- Yitbarek, A.; Razack, M.; Ayenew, T.; Zemedagegnehu, E.; Azagegn, T. Hydrogeological and hydrochemical framework of Upper Awash River basin, Ethiopia: With special emphasis on inter-basins groundwater transfer between Blue Nile and Awash Rivers. *J. Afr. Earth Sci.* **2012**, *65*, 46–60. [[CrossRef](#)]
- Devlin, J.F.; Tsofiias, G.; McGlashan, M.; Schillig, P. An inexpensive multilevel array of sensors for direct ground water velocity measurement. *Gr. Water Monit. Remediat.* **2009**, *29*, 73–77. [[CrossRef](#)]
- Bakx, W.; Bense, V.F.; Karaoulis, M.; Oude Essink, G.H.P.; Bierkens, M.F.P. Measuring groundwater flow velocities near drinking water extraction wells in unconsolidated sediments. *Water* **2023**, *15*, 2167. [[CrossRef](#)]
- Li, F.; Dai, C.; Lei, H. Review of groundwater flow velocity measurement method. *Trans. Geotherm. Resour. Counc.* **2019**, *43*, 723–734.
- Devlin, J.F. *Groundwater Velocity*; The Groundwater Project; University of Guelph: Guelph, ONT, Australia, 2020.
- Chae, H.; Nagano, K.; Sakata, Y.; Katsura, T.; Kondo, T. Estimation of fast groundwater flow velocity from thermal response test results. *Energy Build.* **2020**, *206*, 109571. [[CrossRef](#)]
- Ahmad, M.; Tariq, J.A.; Rafique, M.; Iqbal, N.; Choudhry, M.A.; Qureshi, R.M. *Measurement of Groundwater Flow Velocity At Chashnupp Unit-2 Site Using Radiotracer Technique*; Pakistan Institute of Nuclear Science and Technology: Islamabad, Pakistan, 2008.
- Englert, A. Measurement, Estimation and Modelling of Groundwater Flow Velocity at Krauthausen Test Site. Ph.D. Thesis, Aachen University, Aachen, Germany, 2003.
- Lile, O.B.; Morris, M.; Ronning, J.S. Estimating groundwater flow velocity from changes in contact resistance during a saltwater tracer experiment. *Appl. Geophys.* **1997**, *38*, 105–114. [[CrossRef](#)]
- Medici, G.; West, L.J.; Banwart, S.A. Groundwater flow velocities in a fractured carbonate aquifer-type: Implications for contaminant transport. *J. Contam. Hydrol.* **2019**, *222*, 1–16. [[CrossRef](#)] [[PubMed](#)]
- Drost, W.; Klotz, D.; Koch, A.; Moser, H.; Neumaier, F.; Rauert, W. Point dilution methods of investigating ground water flow by means of radioisotopes. *Water Resour. Res.* **1968**, *4*, 125–146. [[CrossRef](#)]
- Brouye, S. Modeling tracer injection and well-aquifer interactions: A new mathematical and numerical approach. *Water Resour. Res.* **2003**, *39*, 1070.
- Hatfield, K.; Annable, M.; Cho, J.; Rao, P.S.C.; Klammner, H. A direct passive method for measuring water and contaminant fluxes in porous media. *J. Contam. Hydrol.* **2004**, *75*, 155–181. [[CrossRef](#)]
- Osorno, T.C.; College, S.N. Development and Testing of an In-well Point Velocity Probe for Preliminary Site Characterization. Master's Thesis, University of Kansas, Lawrence, KS, USA, 2016.
- Kearl, P.M.; Roemer, K.; Rogoff, E.B.; Renn, R.M. Characterization of a fractured aquifer using the colloidal borescope. *Adv. Environ. Res.* **1998**, *3*, 49–57.

27. Liu, B.; Yan, G.; Ma, Y.; Scheuermann, A. Measurement of In-Situ Flow Rate in Borehole by Heat Pulse Flowmeter: Field-Case Study and Reflection. *Geosciences* **2023**, *13*, 146. [[CrossRef](#)]
28. Essouayed, E.; Annable, M.D.; Momtbrun, M.; Atteia, O. An innovative tool for groundwater velocity measurement compared with other tools in laboratory and field tests. *J. Hydrol. X* **2019**, *2*, 100008. [[CrossRef](#)]
29. Hamada, H. Estimation of groundwater flow rate using the decay of <sup>222</sup>Rn in a well. *J. Environ. Radioact.* **2000**, *47*, 1–13. [[CrossRef](#)]
30. Cook, A.J.; Love, J.C. Dighton Inferring Ground Water flow In Fractured Rock From Dissolved Radon. *Ground Water* **1999**, *37*, 606–610. [[CrossRef](#)]
31. Schubert, M.; Brueggemann, L.; Knoeller, K.; Schirmer, M. Using radon as an environmental tracer for estimating groundwater flow velocities in single-well tests. *Water Resour. Res.* **2011**, *47*, 1–8. [[CrossRef](#)]
32. Al-Madhlom, Q.; Al-Ansari, N.; Abid, B.; Laue, J.; Musa, H. Seepage velocity: Large scale mapping and the evaluation of two different aquifer conditions (silty clayey and sandy). *Hydrology* **2020**, *7*, 60. [[CrossRef](#)]
33. Abdullah, T.O.; Ali, S.S.; Al-ansari, N.A.; Knutsson, S.; Laue, J. Magnitude and Direction of Groundwater Seepage Velocity in Different Soil and Rock Materials. *Engineering* **2020**, *12*, 242–253. [[CrossRef](#)]
34. Mohr, P.; Zanettin, B. The Ethiopian flood basalt province. In *Cont Flood Basalts*; Springer: Berlin/Heidelberg, Germany, 1988; pp. 63–110.
35. Mohr, P.A. Major volcano-tectonic lineament in the Ethiopian Rift System. *Nature* **1967**, *213*, 664–665. [[CrossRef](#)]
36. Kebede, S.; Travi, Y.; Alemayehu, T.; Ayenew, T. Groundwater recharge, circulation and geochemical evolution in the source region of the Blue Nile River, Ethiopia. *Appl. Geochem.* **2005**, *20*, 1658–1676. [[CrossRef](#)]
37. Peccerillo, A.; Donati, C.; Santo, A.P.; Orlando, A.; Yirgu, G.; Ayalew, D. Petrogenesis of silicic peralkaline rocks in the Ethiopian rift: Geochemical evidence and volcanological implications. *J. Afr. Earth Sci.* **2007**, *48*, 161–173. [[CrossRef](#)]
38. Woldegabriel, G.; Aronson, J.L.; Walter, R.C. Geology, geochronology, and rift basin development in the central sector of the Main Ethiopia Rift. *Bull. Geol. Soc. Am.* **1990**, *102*, 439–458. [[CrossRef](#)]
39. Ayenew, T.; Demlie, M.; Wohnlich, S. Hydrogeological framework and occurrence of groundwater in the Ethiopian aquifers. *J. Afr. Earth Sci.* **2008**, *52*, 97–113.
40. Berehanu, B.; Azagegn, T.; Ayenew, T.; Masetti, M. Inter-Basin Groundwater Transfer and Multiple Approach Recharge Estimation of the Upper Awash Aquifer System. *J. Geosci. Environ. Prot.* **2017**, *5*, 76–98. [[CrossRef](#)]
41. Demlie, M.; Wohnlich, S.; Wisotzky, F.; Gizaw, B. Groundwater recharge, flow and hydrogeochemical evolution in a complex volcanic aquifer system, central Ethiopia. *Hydrogeol. J.* **2007**, *15*, 1169–1181. [[CrossRef](#)]
42. Kebede, S.; Travi, Y.; Asrat, A.; Alemayehu, T.; Ayenew, T.; Tessema, Z. Groundwater origin and flow along selected transects in Ethiopian rift volcanic aquifers. *Hydrogeol. J.* **2008**, *16*, 55–73. [[CrossRef](#)]
43. Abebe, T.; Mazzarini, F.; Innocenti, F.; Manetti, P. The Yerer-Tullu Wellel volcanotectonic lineament: A transtensional structure in central Ethiopia and the associated magmatic activity. *J. Afr. Earth Sci.* **1998**, *26*, 135–150. [[CrossRef](#)]
44. Boccaletti, M.; Bonini, M.; Mazzuoli, R.; Abebe, B.; Piccardi, L.; Tortorici, L. Quaternary oblique extensional tectonics in the Ethiopian Rift (Horn of Africa). *Tectonophysics* **1998**, *287*, 97–116. [[CrossRef](#)]
45. Ayalew, D.; Barbey, P.; Marty, B.; Reisberg, L.; Yirgu, G.; Pik, R. Source, genesis, and timing of giant ignimbrite deposits associated with Ethiopian continental flood basalts. *Geochim. Cosmochim. Acta* **2002**, *66*, 1429–1448. [[CrossRef](#)]
46. Alemu, M. Comparative Analysis of the Effects of Land Use/Land Cover Changes on Hydrology and Sedimentation: The Case of Wabeand Meki Catchments, Central Ethiopia. Ph.D. Thesis, Addis Ababa University, Addis Ababa, Ethiopia, 2017.
47. Furi, W.; Razack, M.; Abiye, T.A.; Ayenew, T.; Legesse, D. Fluoride enrichment mechanism and geospatial distribution in the volcanic aquifers of the Middle Awash basin, Northern Main Ethiopian Rift. *J. Afr. Earth Sci.* **2011**, *60*, 315–327. [[CrossRef](#)]
48. Abbate, E.; Bruni, P.; Sagri, M. Geology of Ethiopia: A Review and Geomorphological Perspectives. In *Landscapes and Landforms of Ethiopia*; Billi, P., Ed.; World Geomorphological Landscapes; Springer: Berlin/Heidelberg, Germany, 2015; pp. 33–64.
49. Beccaluva, L.; Bianchini, G.; Natali, C.; Siena, F. Continental flood basalts and mantle plumes: A case study of the Northern Ethiopian Plateau. *J. Petrol.* **2009**, *50*, 1377–1403. [[CrossRef](#)]
50. Kieffer, B.; Arndt, N.; Lapierre, H.; Bastien, F.; Bosch, D.; Pecher, A.; Yirgu, G.; Ayalew, D.; Weis, D.; Jerram, D.A.; et al. Flood and shield basalts from Ethiopia: Magmas from the African superswell. *J. Petrol.* **2004**, *45*, 793–834. [[CrossRef](#)]
51. Lebas, M.J.; Mohr, P.A. Tholeiite from the Simien alkali basalt centre, Ethiopia. *Geol. Mag.* **1970**, *107*, 523–529. [[CrossRef](#)]
52. Sembroni, A.; Faccenna, C.; Becker, T.W.; Molin, P.; Abebe, B. Long-term, deep-mantle support of the Ethiopia-Yemen Plateau. *Tectonics* **2016**, *35*, 469–488.
53. Neuman, S.P. Analysis of pumping test data from anisotropic unconfined aquifers considering delayed gravity response. *Water Resour. Res.* **1975**, *11*, 329–342. [[CrossRef](#)]
54. Theis, C.V. The relation between the lowering of the Piezometric surface and the rate and duration of discharge of a well using ground-water storage. *Eos Trans. Am. Geophys. Union* **1935**, *16*, 519–524. [[CrossRef](#)]
55. Fitts, C.R. *Groundwater Science*; Elsevier: Amsterdam, The Netherlands, 2013; ISBN 9780123847058.
56. Ahuja, R.; Cassel, K.; Bruce, R.; Barnes, B. Evaluation of Spatial Distribution of Hydraulic Conductivity Using Effective Porosity Data. *Soil Sci.* **1989**, *148*, 404–411. [[CrossRef](#)]
57. Wilkinson, J.M. The application and revision of a new relationship to calculate effective porosity from specific capacity on a well database in the Pacific Northwest. *Hydrol. Res. Lett.* **2012**, *103*, 98–103. [[CrossRef](#)]

58. Razack, M.; Huntley, D. Assessing Transmissivity from Specific Capacity in a Large and Hetrogeneous Alluvial Aquifer. *Ground Water* **1991**, *29*, 856–861. [[CrossRef](#)]
59. Gupta, R.S. *Hydrology & Hydraulic Systems Hydrology & Hydraulic Systems*; Waveland Press: Long Grove, IL, USA, 2017; ISBN 9781478630913.
60. Environmental Systems Research Institute (ESRI). *Darcy Velocity*, ESRI: Tysons, VA, USA, 2015.
61. Maurice, L.; Taylor, R.G.; Tindimugaya, C.; MacDonald, A.M.; Johnson, P.; Kaponda, A.; Owor, M.; Sanga, H.; Bonsor, H.C.; Darling, W.G.; et al. Characteristics of high-intensity groundwater abstractions from weathered crystalline bedrock aquifers in East Africa. *Hydrogeol. J.* **2019**, *27*, 459–474. [[CrossRef](#)]
62. Cherry, J. Groundwater monitoring: Some deficiencies and opportunities. In *Hazardous Waste Site Investigations; Towards Better Decisions, Proceedings of the 10th ORNL Life Science Symposium, Gatlinburg, TN, USA, 21–24 May 1990*; CRC Press: Boca Raton, FL, USA, 1990.
63. Aley, T. *Groundwater Tracing Handbook*; Ozark Underground Laboratory: Protem, MO, USA, 2002; Volume 65733, p. 35.
64. Morris, D.A.; Johnson, A.I. Summary of Hydrologic and Physical Properties of Rock and Soil Materials, as Analyzed by the Hydrologic Laboratory of the U.S. Geological Survey. *USA Geol. Surv.* **1967**, *1839-D*, 1948–1960.
65. Hall, S.H. Single Well Tracer Tests in Aquifer Characterization. *Groundw. Monit. Remediat.* **1993**, *13*, 118–124. [[CrossRef](#)]
66. Piccinini, L.; Fabbri, P.; Pola, M. Point dilution tests to calculate groundwater velocity: An example in a porous aquifer in northeast Italy. *Hydrol. Sci. J.* **2016**, *61*, 1512–1523. [[CrossRef](#)]
67. Poulsen, D.L.; Cook, P.G.; Simmons, C.T.; McCallum, J.M.; Noorduijn, S.L.; Dogramaci, S. A constant rate salt tracer injection method to quantify pumped flows in long-screened or open borehole wells. *J. Hydrol.* **2019**, *574*, 408–420. [[CrossRef](#)]
68. Vienken, T.; Huber, E.; Kreck, M.; Huggenberger, P.; Dietrich, P. How to chase a tracer—Combining conventional salt tracer testing and direct push electrical conductivity profiling for enhanced aquifer characterization. *Adv. Water Resour.* **2017**, *99*, 60–66. [[CrossRef](#)]
69. Matsumoto, S.; Machida, I.; Hebig, K.H.; Zeilfelder, S.; Ito, N. Estimation of very slow groundwater movement using a Single-Well Push-Pull test. *J. Hydrol.* **2020**, *591*, 125676. [[CrossRef](#)]
70. Labaky, W.; Devlin, J.F.; Gillham, R.W. Field comparison of the point velocity probe with other groundwater velocity measurement methods. *Water Resour. Res.* **2009**, *45*, 1–9. [[CrossRef](#)]
71. Mazor, E.; Nativ, R. Hydraulic calculation of groundwater flow velocity and age: Examination of the basic premises. *J. Hydrol.* **1992**, *138*, 211–222. [[CrossRef](#)]
72. Abdullah, T.; Ali, S.S.; Al-Ansari, N.; Knutsson, S. Seepage Velocity of Different Groundwater Aquifers in Halabja Saidasadiq Basin—NE of Iraq. In *Proceedings of the Environmental Science and Engineering, Virtual, 5–7 June 2021*.

**Disclaimer/Publisher’s Note:** The statements, opinions and data contained in all publications are solely those of the individual author(s) and contributor(s) and not of MDPI and/or the editor(s). MDPI and/or the editor(s) disclaim responsibility for any injury to people or property resulting from any ideas, methods, instructions or products referred to in the content.